Computers & Geosciences ▮ (▮▮▮▮) ▮▮▮–▮▮▮

Contents lists available at ScienceDirect

Computers & Geosciences

journal homepage: www.elsevier.com/locate/cageo

On the simulation of continuous in scale universal multifractals, part I: Spatially continuous processes

S. Lovejoy [a,b,*], D. Schertzer [c,d]

[a] Department of Physics, McGill University, 3600 University St., Montreal, Que., Canada
[b] GEOTOP, UQAM, CP 8888, Succ. Centre Ville, Montreal, Que., Canada H3C 3P8
[c] Université Paris-Est, ENPC/CEREVE, 77455, Marne-la-Vallee Cedex 2, France
[d] Météo France, 1 Quai Branly, 75007 Paris, France

ARTICLE INFO

Article history:
Received 10 October 2008
Received in revised form
9 January 2010
Accepted 1 April 2010

Keywords:
Multifractals
Fractals
Scaling
Turbulence
Numerical simulations

ABSTRACT

Cascade processes generically lead to multifractal fields and have been used for simulating turbulent systems – including clouds, rain, temperature, passive scalars and the wind – as well as for solid earth fields, such as rock density, magnetization and topography. In spite of their importance, most applications use primitive discrete scale ratio processes, which singularize scales which are integer powers of integers. Realistic simulations are continuous in scale, but suffer from strong "finite size effects" i.e. deviations from pure power law scaling, which can take surprisingly large ranges of scale to disappear. In this two part series, we quantify and show the origin of the problem and quantify its magnitude (part I), while in part II we show how to largely overcome it and give a *Mathematica* code for the corresponding simulations for causal and acausal space-time simulations.

1. Introduction: first generation multifractal models: discrete in scale

In the past 25 years, there has been an explosion of interest in multifractals and in the generic multifractal process: the multiplicative cascade. In spite of this motivation, there has been surprisingly little attention paid to the numerical modeling of realistic multifractal processes which are continuous in scale. Indeed nearly all the simulations in the literature are of "first generation" type, they are discrete in scale (Novikov and Stewart, 1964; Yaglom, 1966; Mandelbrot, 1974), they almost invariably use the discrete cascade ratio $\lambda_0=2$.

These largely pedagogical discrete in scale models are constructed by iteratively dividing large structures ("eddies") into disjoint daughter "subeddies," each reduced in scale by the integer ratio λ_0. The smaller eddies have intensities which are equal to those of their parents, multiplicatively weighted by independently and identically distributed random factors. They yield visually weird, highly artificial simulations (see e.g. Fig. 1a). Other key limitations of these standard "toy model" cascades include (a) isotropy (self-similarity; although limited self-affine extensions are possible (Schertzer and Lovejoy, 1985b)) and (b) left-right symmetry (which precludes causal processes). In addition, most multifractal models are of scale by scale conserved cascade quantities, whereas the observables typically have exponents with an extra linear term. A somewhat different but still discrete in scale multifractal simulation method is based on iterated function systems (Levy-Véhel et al., 1995; Basu et al., 2004). Probably the most sophisticated discrete in scale approach is the Markov-Switching Multifractal (MSM) simulation method; it is available only for pure (1-D) time series (Calvet and Fisher, 2001; Calvet and Fisher, 2008). This model involves causal random transitions, but is still based on iterating a finite fundamental scale ratio, so that it is not yet continuous in scale. We could also mention "bounded cascades" (Cahalan, 1994), but these are not really multifractal.

While "second generation" continuous in scale multifractal processes based on stable (Levy) random variables were proposed over 20 years ago (Schertzer and Lovejoy, 1987), in many cases they converge frustratingly slowly to their theoretical (large scale ratio) form. This slow convergence has somewhat diminished the appeal of these continuous in scale models. In the first part of this paper, we consider spatially continuous processes which are also continuous in scale and point out the nontrivial origin of the problem. In part II, we consider the additional effects of spatial discretisation and propose improvements, which make the models much more attractive.

Part I is structured as follows. In Section 2, we review the basic continuous in scale process cascade properties, its normalization

* Corresponding author at: Department of Physics, McGill University, 3600 University St., Montreal, Que., Canada. Tel.: +1 514 398 6537.
E-mail address: lovejoy@physics.mcgill.ca (S. Lovejoy).

0098-3004/$ - see front matter © 2010 Published by Elsevier Ltd.
doi:10.1016/j.cageo.2010.04.010

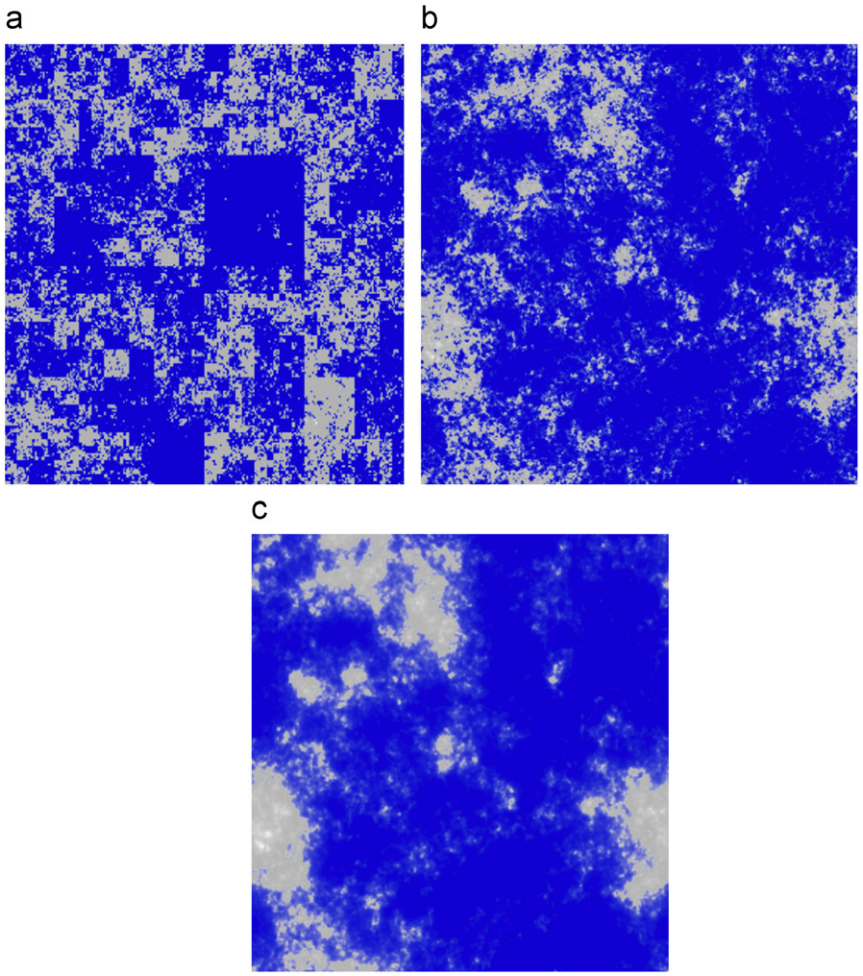

Fig. 1. (a) Discrete in scale simulation, scale ratio 2, $\lambda=2^9$, $\alpha=1.8$, $C_1=0.1$. Grey scale proportional to the log of the field, low values are colored blue to improve contrast. (b) Corresponding continuous in scale simulation, using continuous in scale method with $\Delta x^{-D/\alpha}$ corrections, as described in part II (with $D=2$). (c) Same as Fig. 1b, but with an additional fractional integration of order $H=1/3$ (a scale invariant smoothing); to simulate a turbulent passive scalar density.

and one point statistics. In Section 3, we consider the behaviour of the second characteristic function (SCF) of the generator of the autocorrelation function showing that the main correction to the dominant $\log \Delta x$ behaviour is a slowly decaying $\Delta x^{-D/\alpha}$ term. In part II, we consider the additional complications arising from the spatial discretisation used in numerical work and show how to correct for the $\Delta x^{-D/\alpha}$ bias. In Section 4, we conclude. We have also included several appendices (all of which are collected at the end of part II) with various technical details, including a Mathematica code. An overview of the theory and applications to the atmosphere can be found in Lovejoy and Schertzer, 2010b.

2. Continuous in scale universal multifractal cascades: deviations from pure power law scaling

2.1. Basic statistical properties of cascades

If we denote the scale by scale conserved multifractal field by ε_λ, it has statistics of the form

$$\langle \varepsilon_\lambda^q \rangle = \lambda^{K(q)} \tag{1}$$

where λ=(largest scale)/(smallest resolution scale) is the resolution, the scaling moment function $K(q)$ determines the statistical properties of the process and "$<.>$" indicates statistical (ensemble) averaging. $K(q)$ is the (base λ, Laplace) second characteristic function (SCF, sometimes called the "cumulant generating function") of the generator Γ_λ as can be seen by taking base λ logs of Eq. (1)

$$K(q) = \log_\lambda \langle e^{\Gamma_\lambda q} \rangle; \quad \Gamma_\lambda = \log \varepsilon_\lambda \tag{2}$$

The scale by scale conservation of the cascade is expressed by $\langle \varepsilon_\lambda \rangle = 1$ implying $K(1)=0$; it is necessary for the convergence in the small scale limit. If we denote by Λ the maximum scale ratio of the model, then Fig. 1a shows the result of a spatially discrete and discrete in scale model built up through $n=9$ cascade steps each of ratio $\lambda_0=2$; the total range is $\Lambda=\lambda_0^n$. If we consider the discrete model at intermediate scale ratios $1<\lambda<\Lambda$, then Eq. (1) only holds for the integer scales $\lambda=\lambda_0^m$ ($0\le m\le n$ is an integer). These special scales give rise to unsightly linear artifacts in the simulations (e.g. Fig. 1a). In contrast, Fig. 1b shows a spatially discrete, but continuous in scale simulation in which Eq. (1) (nearly) holds for all the intermediate scale ratios $\lambda<\Lambda$ (with the same $K(q)$). Clearly, since empirical fields are generally continuous in scale, alternatives to the discrete in scale cascades are necessary for realism.

In addition to being continuous in scale, realistic models of typical observables involve another extra (linear) scaling. For example, the resolution λ velocity fluctuations (Δv_λ) in turbulence—vary with λ as $\Delta v_\lambda = \varepsilon_\lambda^a \lambda^{-H}$. If ε is the energy flux and $a=H=1/3$, this is the Kolmogorov law for an isotropic three dimensional turbulence (Kolmogorov, 1941). To model a v field

Please cite this article as: Lovejoy, S., Schertzer, D., On the simulation of continuous in scale universal multifractals, part I: Spatially continuous processes. Computers and Geosciences (2010), doi:10.1016/j.cageo.2010.04.010

with such statistics, it suffices to take a fractional integral (power law filter) of order H of ε^a; see (Schertzer and Lovejoy, 1987) for this "fractionally integrated flux" (FIF) model for the observables (see Fig. 1c). Finally, realistic systems are rarely if ever isotropic so that we generally require anisotropic ("Generalized") scale invariance, in which the usual isotropic notions of scale are replaced by anisotropic ones, the vector norms used in the convolutions are replaced by scale functions (Schertzer and Lovejoy, 1985a). For examples, see the site: http://www.physics.mcgill.ca/~gang/multifrac/index.htm.

The basic simulation method is to directly construct a continuous in scale band-limited noise Γ_λ and then to exponentiate it to obtain ε_λ (Eq. (2)). Since Γ_λ is taken to be a continuous in scale stochastic process, it must be "infinitely divisible". The original proposal for such continuous in scale cascades (Schertzer and Lovejoy, 1987) used Levy processes for the generators, but other infinitely divisible generators, such as Poisson processes can also be used (She and Levesque, 1994); see (Schertzer et al., 1995) for a comparison and discussion). The Levy generators Γ_λ are particularly useful since they are the stable, attractive limits of additive processes; $\varepsilon_\lambda = e^{\Gamma_\lambda}$ are thus referred to as "universal multifractals". This universality is a consequence of the central limit theorem applied to the (additive) generator Γ_λ and corresponds to a multiplicative central limit theorem for the process ε_λ; see (Schertzer and Lovejoy, 1997) for discussion and debate). The resulting two parameter universal form for $K(q)$ is

$$K(q) = \frac{C_1}{\alpha-1}(q^\alpha - q); \quad 0 \le \alpha \le 2; \quad 0 < C_1 < D \tag{3}$$

where α is the Levy index characterizing the degree of multifractality and C_1 is the codimension of the mean characterizing the sparseness of the mean field. D is the dimension of space, and for $\alpha < 2$, $K(q)$ diverges for $q > 0$. We could also mention that in the case $\alpha = 1$: using L'Hôpital's rule, we must take the limit $\alpha \to 1$ of Eq. (3) to obtain

$$K(q) = C_1 q \log q; \quad \alpha = 1; \quad 0 < C_1 < D \tag{4}$$

Fig. 2 shows various examples in one and two dimensions showing the effect of changing α and C_1.

Although most empirical estimates of the parameters α, C_1 have been made for atmospheric quantities (see e.g. Lovejoy et al., 2009b results in the vertical and Lovejoy et al., 2010 in the horizontal, for a review in the atmosphere, Lovejoy and Schertzer, 2010a including satellite radiances, e.g. Laferrière and Gaonac'h, 1999; Lovejoy et al., 2009a), some solid-earth results exist, notably for the topography, surface magnetic field, and ore concentration, (see the review Lovejoy and Schertzer, 2007; Cheng and Agterberg, 1996). Although this is not the place to discuss in detail the now numerous results, a fairly general finding is that with few exceptions, $2 > \alpha > 1.5$ and $C_1 < 0.3$.

2.2. The internal cascade structure

Various numerical details and examples of simulations of continuous in scale isotropic (self-similar) multifractals were given in Schertzer and Lovejoy (1987) and Wilson et al. (1991). Marsan et al. (1996) showed how to extend the framework to causal (space-time) processes, and Pecknold et al. (1996); Pecknold et al. (1997) developed extensions to anisotropic multifractal processes needed for example to take into account atmospheric stratification. As we detail in Section 3, the basic method for simulating Γ is to fractionally integrate a Levy noise, i.e. to convolve it with a singularity. While this method works for large enough scale ranges (i.e. it yields simulations with statistics satisfying Eqs. (1) and (3) for large enough λ), there are significant deviations at small scales ("finite size effects"), especially for $\alpha > 1$ which is the most empirically relevant range. In order to get an idea of the importance of these deviations, consider the theoretical form of the normalized autocorrelation function $R_\lambda(\underline{\Delta x})$ for isotropic cascades

$$R_\lambda(\underline{\Delta x}) = \frac{\langle \varepsilon_\lambda(\underline{x})\varepsilon_\lambda(\underline{x}-\underline{\Delta x})\rangle}{\langle \varepsilon_\lambda^2 \rangle} = |\underline{\Delta x}|^{-K(2)}; \quad |\underline{\Delta x}| \ge 1 \tag{5}$$

(as derived on discrete in scale cascades by (Monin and Yaglom, 1975)), $\underline{x}$, $\underline{\Delta x}$ are D dimensional position vectors and lags, respectively. The above uses the convention that the process is developed over the range of scales from λ down to 1 unit, so that $R_\lambda(1) = 1$ (see Section 2.3 on this). $K(2)$ appears because the autocorrelation is a $q = 2$ order statistic. Since the spectrum is the Fourier transform of the autocorrelation function, we find that for wavenumber $k = |\underline{k}|$, the power spectrum $E(k)$ of ε_λ has the scaling form

$$E(k) \approx k^{-\beta}; \quad \beta = 1 - K(2) \tag{6}$$

Fig. 3a shows the power spectrum of the process for $\alpha = 2$ compensated by dividing by the theoretical $k^{-\beta}$, so that the theoretically expected spectral scaling leads to horizontal straight lines on the log–log plots. From the figure, we can see that the pure (power law) fractional integration takes nearly a factor of 10^3 in scale to completely converge (the largest wavenumber for a 2^{14} point long series is $k = 2^{13} \approx 10^4$); Fig. 3b shows the same basic result for smaller α values. Although the rate of convergence improves as α decreases from 2, it is noticeable for all α. Also shown in the figure are the corresponding spectra of the processes obtained using the improved simulation techniques described in this paper. It can be seen that although the spectral results are still not perfect that they are significantly better. Fig. 4 compares samples of the original process and with the various corrections discussed. Although the visible differences in the realizations are apparently not so large, the statistics as revealed by various scale by scale analyses are still quite biased at small scales.

2.3. Moment analysis using dressed fluxes

A simulation of a cascade process proceeding over a scale range factor Λ has statistics at the finest simulated scale, which indeed obey (or as here, nearly obey) Eq. (1) with $\lambda = \Lambda$, i.e. $\langle \varepsilon_\Lambda^q \rangle = \Lambda^{K(q)}$. This means that the variability at the smallest resolution is of the expected form, yet the simulations may nevertheless not be completely satisfactory, since the internal statistics at larger scales (smaller scale ratios, $\lambda < \Lambda$, smaller wave numbers $k < \Lambda$) may be biased. We saw this in the previous section: by using spectral analysis, we found that the spectrum for wavenumbers $k < \Lambda$ was only of the theoretically expected power law form for $k \ll \Lambda$. However, spectral analysis is a second order statistic, it is important to consider the statistics at scales $\lambda < \Lambda$ for all orders q, not just $q = 2$.

In order to study the larger scale statistics (i.e. $\lambda < \Lambda$), it is convenient to estimate the simulated λ scale fluxes by integrating over the corresponding scale (i.e. by degrading the resolution by a scale ratio Λ/λ)

$$\varepsilon_{\lambda,\Lambda,(d)}(j) = \left(\frac{\Lambda}{\lambda}\right) \sum_{i=1}^{\Lambda/\lambda} \varepsilon_\Lambda\left(\frac{(j-1)\Lambda}{\lambda} + i\right) \tag{7}$$

In Eq. (7), we have taken the realizations $\varepsilon_\Lambda(i)$ to be defined over the integer coordinates $1 \le i \le \Lambda$, so that the length of the realization is equal to the largest scale, and the smallest scale ($=1$) corresponds to the largest scale ratio (Λ). Similarly, with the definition from Eq. (7), the low resolution, "dressed" $\varepsilon_{\lambda,\Lambda,(d)}$ is defined over integer coordinates $1 \ge j \ge \lambda$. We note that $\varepsilon_{\lambda,\Lambda,(d)}(j)$ has the same resolution as a pure (non-summed/integrated)

Please cite this article as: Lovejoy, S., Schertzer, D., On the simulation of continuous in scale universal multifractals, part I: Spatially continuous processes. Computers and Geosciences (2010), doi:10.1016/j.cageo.2010.04.010

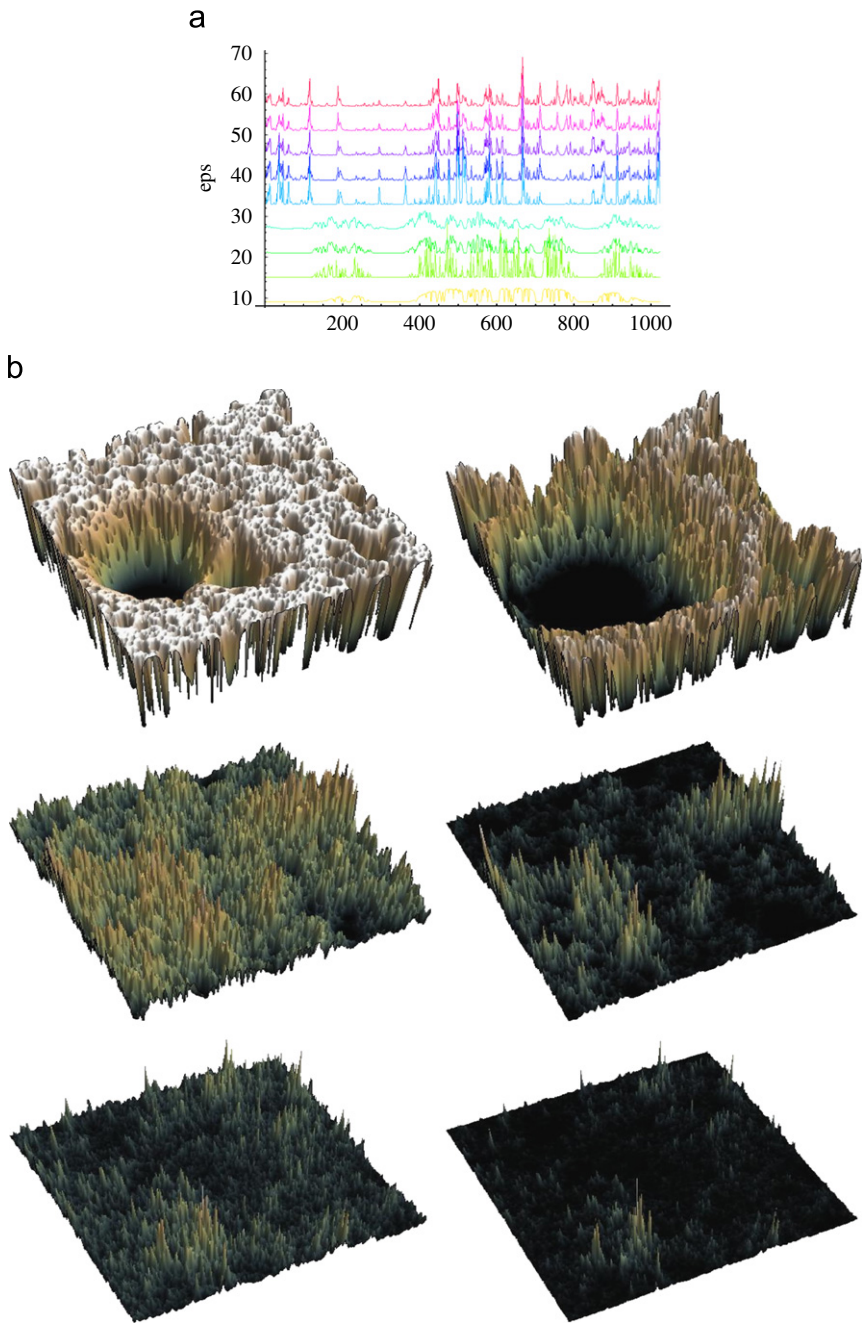

Fig. 2. (a) Multifractal simulations $C_1=0.1$ and $\alpha=0.3, 0.5, \ldots, 1.9$ from bottom to top, offset for clarity (same random seed). (b) Isotropic realizations in two dimensions with $\alpha=0.4, 1.2, 2$, (top to bottom) and $C_1=0.05, 0.15$ (left to right). Random seeds are fixed so as to make clear change in structures as parameters are changed. Low α simulations are dominated by frequent very low values; "Levy holes". Vertical scales are not the same.

"bare" process ε_λ with scale ratio λ; we compare the two below. For simplicity, we consider 1-D processes, but the extensions to the higher dimensions are straightforward.

Note that this convention that the smallest spatial scale is unity is convenient in our present context, but is not standard. Usually when studying cascades, we are interested in the statistics as the resolution of a cascade defined on the unit interval is progressively increased with the smallest scale resolution$=1/\Lambda$ decreasing with Λ rather than the inner (smallest) scale being fixed at unity and the external scale$=\Lambda$. Here, however, we are more interested in making spatially discrete simulations with a fixed outer scale, intermediate resolution Greek lambda behaviour by integrating/summing simulations whose spatial resolution are unity.

Since the dressed $\varepsilon_{\lambda,\,\Lambda,(d)}(j)$ still has variability from the larger scales (smaller scale ratios), we see that the difference between the bare and dressed processes at a resolution λ is that the former has some extra variability, due to the parts of the process which are averaged out ("dressed") in Eq. (7). As shown in (Schertzer and Lovejoy, 1987) with the help of "trace moments," the theoretical relation between the dressed process and the corresponding bare process at the resolution λ is

$$\varepsilon_{\lambda,\Lambda(d)} = \varepsilon_\lambda \varepsilon_{\lambda,\Lambda(h)} \tag{8}$$

where the "hidden" flux $\varepsilon_{\lambda,\Lambda(h)}$ is a statistically independent multiplier "hidden" by the integration/summing. It has the property that in the large Λ limit, it implies the divergence of

Please cite this article as: Lovejoy, S., Schertzer, D., On the simulation of continuous in scale universal multifractals, part I: Spatially continuous processes. Computers and Geosciences (2010), doi:10.1016/j.cageo.2010.04.010

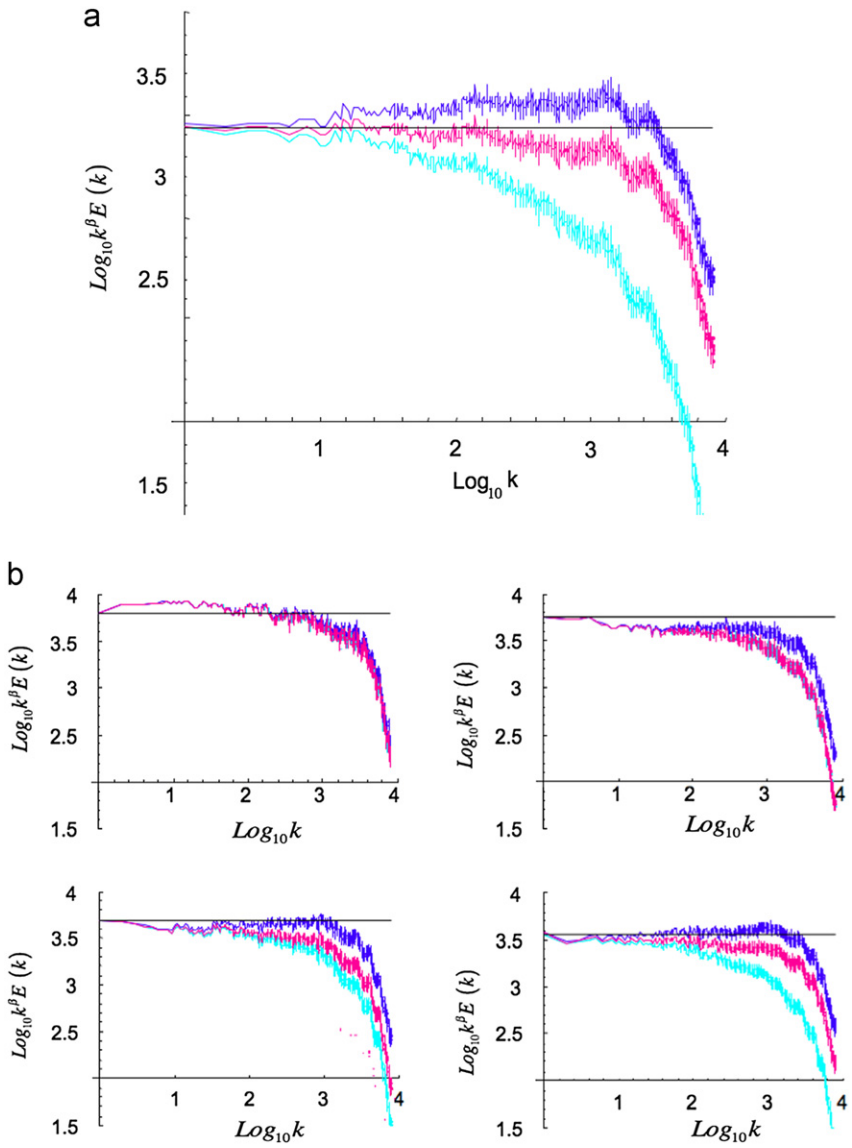

Fig. 3. (a) Compensated power spectrum for 200 realizations of the $\alpha=2$, $C_1=0.2$ process (with $\Lambda=2^{14}$). Compensation uses the theoretical power law form $k^{-\beta}$ with $\beta=K(2)=(C_1/(\alpha-1))(2^{\alpha}-2)$. Cyan is result for pure singularity, red corrected for $\Delta x^{-1/\alpha}$ terms (Section 5.1) and dark blue the "Δx^{-1}" method (Appendix D). (b) Same as Fig. 3a, but for $\alpha=0.4$, 0.8, 1.2, 1.6 (top to bottom, left to right). For $\alpha=0.4$, 0.8, pure power law $\Delta x^{-1/\alpha}$ and corrected power law (cyan and red) are nearly superposed. (For interpretation of the references to color in this figure legend, the reader is referred to the web version of this article.)

statistical moments

$$\lim_{\Lambda\to\infty}\langle\varepsilon^{q}_{\lambda,\Lambda(h)}\rangle=O(1);\quad q<q_D$$
$$\lim_{\Lambda\to\infty}\langle\varepsilon^{q}_{\lambda,\Lambda(h)}\rangle\to\infty;\quad q>q_D \tag{9}$$

where the critical q_D satisfies the implicit equation $C(q_D)=D$, (D is the dimension of the "dressing" $D=1$ here) and $C(q)$ is the strictly decreasing "codimension" function defined by

$$C(q)=\frac{K(q)}{q-1} \tag{10}$$

Equivalently, Eqs. (8) and (9) imply

$$\langle\varepsilon^{q}_{\lambda,\infty(d)}\rangle\approx\lambda^{K(q)};\quad q<q_D$$
$$\langle\varepsilon^{q}_{\lambda,\infty(d)}\rangle=\infty;\quad q>q_D \tag{11}$$

where the "$\approx$" sign indicates equality to within slowly varying factors, i.e. it indicates the leading scaling behaviour. The interpretation of Eqs. (9) and (11) is that the hidden random variables $\varepsilon_{\lambda,\Lambda(h)}$ are typically of order unity, but from time to time have huge excursions, such that their higher moments diverge. This implies that most bare and dressed fluxes are "typically" close to each other, so that for moments $q<q_D$, they have the same scaling behaviour.

In order to test the statistics of the simulations directly on the moments (Eq. (1)), we refer the reader to Fig. 5a,b. Here, the simulations are over a total range of scale $\Lambda=2^{14}$ and $\varepsilon_{\lambda,\Lambda(d)}$ at an intermediate resolution $\lambda<\Lambda$ is estimated by degrading the fine resolution simulation ε_{Λ} with Eq. (7) (for all these simulations, $q_D>5$, so that the divergence is not an issue for the statistics shown). Again we see strong systematic deviations over surprisingly large ranges of scale, especially for the higher order moments. However, this assessment is somewhat misleading since deviations accumulate from small scales to the large scales, so that it is more instructive to examine the process scale by scale. For example, we can look at the change in the moments over

Please cite this article as: Lovejoy, S., Schertzer, D., On the simulation of continuous in scale universal multifractals, part I: Spatially continuous processes. Computers and Geosciences (2010), doi:10.1016/j.cageo.2010.04.010

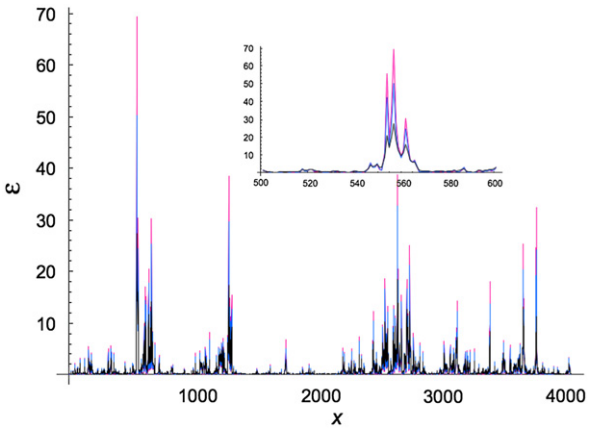

Fig. 4. A simulation with $\alpha=2$, $C_1=0.2$, $l=2^{12}$. Black is raw (pure singularity) simulation, whereas blue is singularity corrected for $\Delta x^{-1/\alpha}$ terms (Section 5.1), and red, uses the "Δx^{-1} method" (part II, Section 4.2). Insert shows a blow up of largest singularity, between $500 \le x \le 600$. (For interpretation of the references to color in this figure legend, the reader is referred to the web version of this article.)

octaves in scale e.g. between resolution λ and 2λ

$$\delta K_\lambda(q) = \frac{\log(\langle \varepsilon^q_{2\lambda,\Lambda(d)} \rangle / \langle \varepsilon^q_{\lambda,\Lambda(d)} \rangle)}{\log 2} \tag{12}$$

Fig. 6a,b shows the results for $\Lambda=2^{14}$ series analyzed with λ increasing by factors of 4. The longest curves are those corresponding to the largest scales (smallest λ). One can see that – with the exception of the last two curves – as one moves to larger and larger scales (smaller λ) that the simulations do indeed become accurate over larger and larger ranges of q, so that part of the reason for the poor performance of the spectrum was that it was a second order moment which required a fairly wide range of scales for convergence. The poor performance at the very largest scales (the two longest curves) is due to another finite size effect discussed below which depends on Λ/λ (no corrections were made for these large scale, smaller amplitude deviations). Also shown in the figures are the significant improvements made by the corrections. Fig. 5b in particular shows that with the proposed $\Delta x^{-1/\alpha}$ corrections, the statistics are very close to those of a cascade with an outer scale somewhat reduced (by a factor of roughly 2 here).

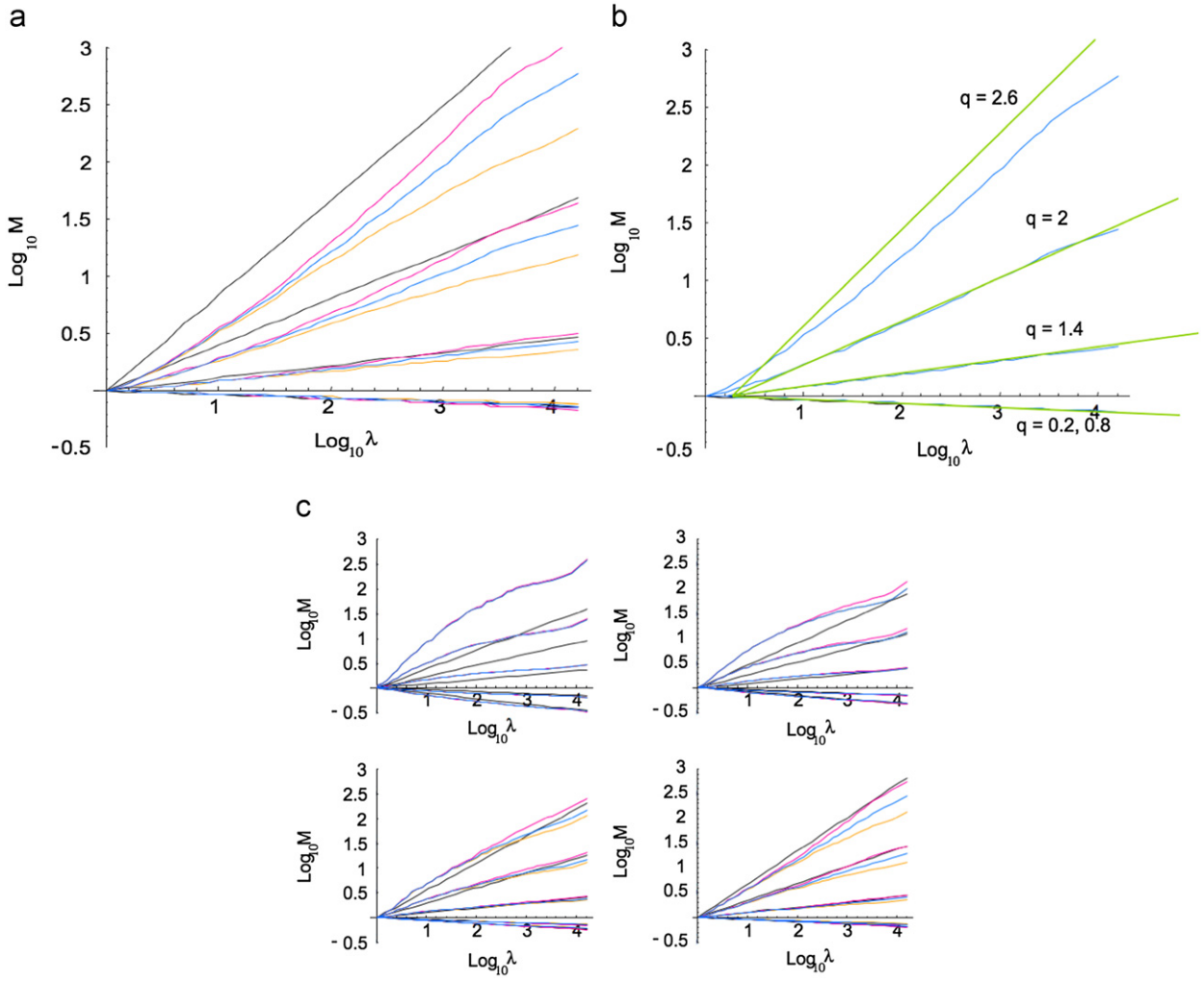

Fig. 5. (a) Various (normalized) moments $M=\langle \varepsilon_\lambda^q \rangle / \langle \varepsilon_\lambda \rangle^q$, for $\alpha=2$ (order 0.2, 0.8, 1.4, 2, 2.6, bottom to top) with pure singularity (orange), $\Delta x^{-1/\alpha}$ corrected (blue) and Δx^{-1} method (red). Theoretically expected behaviour (Eq. (1)) is shown in black. For $\alpha=2$, the $q=0.2$, 0.8 curves are essentially identical as theoretically expected (Eq. (3); they are superposed here). Variability completely disappears at $\lambda=1$, because of the use of microcanonical normalization as discussed in part II. Statistics are based on 200 realizations of a $D=1$ process over a total scale ratio $\Lambda=2^{14}=16{,}384$. (b) $\alpha=2$, $C_1=0.2$, with theoretical $\Delta x^{-1/\alpha}$ corrections compared to theory lines, which go through $\lambda=2$. (c) Same as Fig. 5a, except for $\alpha=0.4$, 0.8, 1.2, 1.6 (upper left to lower right). (For interpretation of the references to color in this figure legend, the reader is referred to the web version of this article.)

Please cite this article as: Lovejoy, S., Schertzer, D., On the simulation of continuous in scale universal multifractals, part I: Spatially continuous processes. Computers and Geosciences (2010), doi:10.1016/j.cageo.2010.04.010

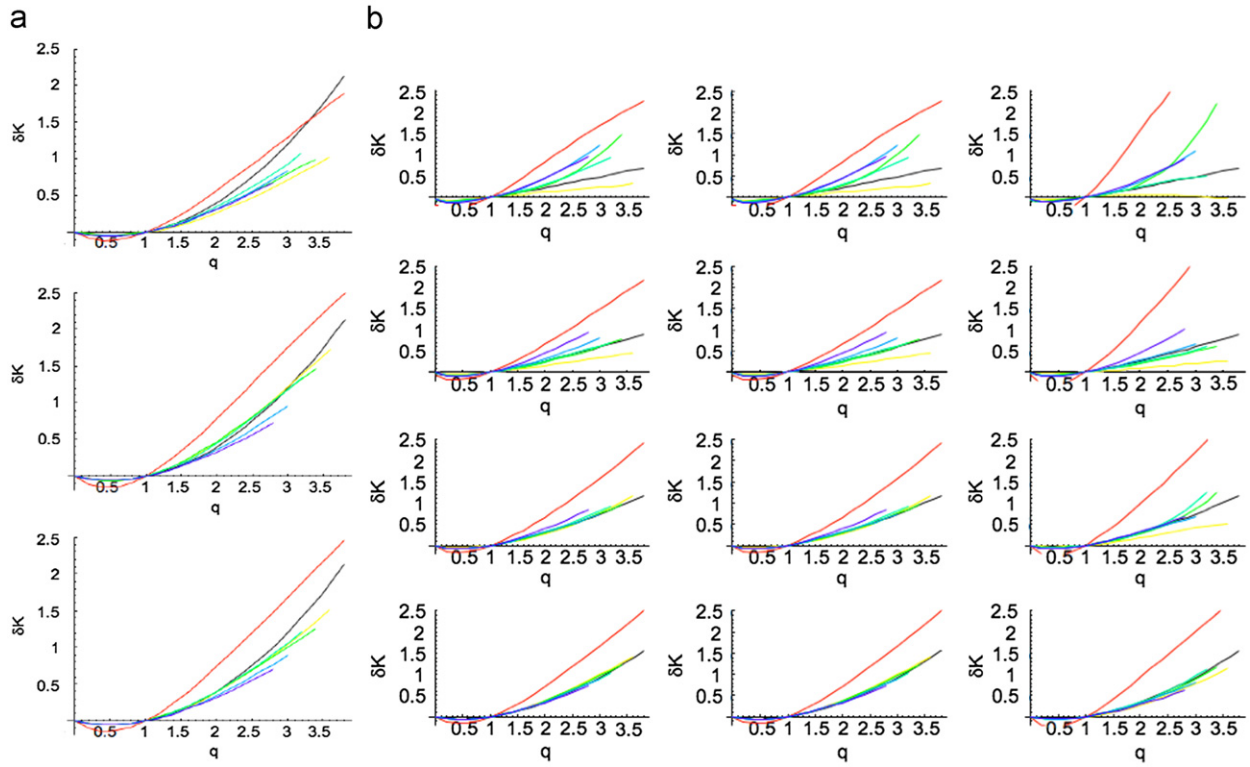

Fig. 6. (a) For $\alpha=2$; averaging over factor 2 in scale, successive curves are separated by factor of 4 in scale. Top to bottom, we have the pure singularity, the Δx^{-1} method (middle) and the $\Delta x^{-1/\alpha}$ correction (bottom). Theoretically expected behaviour (Eq. (3)) is shown in black. Notice Δx^{-1} corrections over-correct for some of the range, whereas $\Delta x^{-\alpha}$ does not. Shortest curve (corresponding to averaging over 2 pixels, $\lambda=2^{13}$) is red, yellow, green are 2^{11}, 2^{9}, green blue: 2^{7}, cyan, 2^{5}, dark blue 2^{3}, purple, 2^{1} ($\lambda=1$ not shown). For clarity, the longer the curve, the larger λ, the smaller the scale. (b) Same as previous, except for $\alpha=0.4$, 0.8, 1.2, 1.6 (top to bottom). Columns, left to right, we have pure singularities (left), the Δx^{-1} (middle) and $\Delta x^{-1/\alpha}$ corrections (right). (For interpretation of the references to color in this figure legend, the reader is referred to the web version of this article.)

In this paper, we argue that the origin of the large deviations can be discerned by considering the two point statistics (the correlation function). We show that in addition to the expected pure power law $\Delta x^{-K(2)}$ behaviour there are $\exp(-A\Delta x^{-D/\alpha})$ residual factors, which die away very slowly and are largest for $\alpha=2$ (A is a constant we derive below). We then propose several methods of reducing/eliminating these biases.

3. Continuous in space, continuous in scale cascades

3.1. Review

3.1.1. One point statistics

As mentioned in the introduction, the basic method of constructing continuous in space, continuous in scale universal multifractals is to start with the generator Γ: (Eq. (2)). We now introduce the "unit" (and extremal) Levy random variable γ_α

$$\begin{aligned} &\langle e^{q\gamma_\alpha}\rangle = e^{q^\alpha/(\alpha-1)}; \quad q\geq 0\\ &\langle e^{q\gamma_\alpha}\rangle = \infty; \qquad\quad q<0; \quad \alpha<2 \end{aligned} \tag{13}$$

(the "$<.>$" sign indicates an ensemble averaging). Note that (a) for $\alpha=2$, we have the familiar Gaussian case and the $q\geq 0$ formula in Eq. (13) is valid for all q, (b) for $\alpha=1$, we have $\langle e^{q\gamma_\alpha}\rangle = e^{q\log q}$ ($q>0$, $=\infty$ otherwise). An extremal Levy random variable A with amplitude $a>0$ and Levy index α therefore satisfies

$$A = a\gamma_\alpha$$

$$\begin{aligned} &\langle e^{qA}\rangle = e^{a^\alpha q^\alpha/\alpha-1}; \quad q\geq 0\\ &\langle e^{qA}\rangle = \infty; \qquad\quad q<0; \quad \alpha<2 \end{aligned} \tag{14}$$

(with corresponding exception for $\alpha=1$). This implies that for the sum of two statistically independent Levy variables A, B we have

$$c^\alpha = a^\alpha + b^\alpha; \quad C = A+B \tag{15}$$

where C is also an extremal Levy with the same α. Eq. (15) expresses the "stability under addition" property of the Levy variables and a, b, c are the corresponding amplitudes. Eq. (15) shows that $\log\langle e^{qF}\rangle$ (the SCF) of the random variables $F=f\gamma_\alpha$ are additive, a property that generalizes to Levy noises; we use this below.

To understand the relation of the extremals to the more general Levy variables l_α with $\alpha<2$, we note that the latter have algebraic tails for both positive and negative values so that

$$\begin{aligned} &\langle |l_\alpha|^q\rangle \to \infty; && q\geq\alpha\\ &p(l_\alpha)\approx A_+ l_\alpha^{-\alpha-1}; && l_\alpha \gg 1\\ &p(l_\alpha)\approx A_-(-l_\alpha)^{-\alpha-1}; && l_\alpha \ll -1 \end{aligned} \tag{16}$$

where p is the probability density and A_+ and A_- are constants that depend on an "asymmetry parameter" (the $\alpha=2$ case is the qualitatively different Gaussian). For symmetric Levy's, $A_+=A_-$; here, we require the maximally asymmetric Levy's without algebraic behaviour for $l\gg 0$.

We can now understand the restriction to extremal Levy variables, since to obtain the cascade process ε, we must exponentiate the generator Γ, which is a linear combination of Levy variables, hence is itself a Levy variable (due to the stability under addition property, Eq. (15)). If – as indicated below – Γ is constructed from Levy's with the long "probability tails" for both $l_\alpha<0$ and $l_\alpha>0$, then the random variable e^{l}_{a} has no converging moments whatsoever: $\langle e^{ql_\alpha}\rangle=\infty$, and hence we would have

Please cite this article as: Lovejoy, S., Schertzer, D., On the simulation of continuous in scale universal multifractals, part I: Spatially continuous processes. Computers and Geosciences (2010), doi:10.1016/j.cageo.2010.04.010

$\langle \varepsilon_\lambda^q \rangle = \langle e^{q\Gamma} \rangle = \infty$ for all q. In order for the process to be normalizable at least positive order moments q must converge, therefore we are forced to restrict our attention to the extremal Levy's γ_α, which are exceptional in that they diverge on only one side (here taken as the negative side); in addition for $\alpha < 1$, they are strictly negative. The qualitative difference between the $\alpha > 1$ and $\alpha < 1$ processes is more apparent, if we consider the corresponding asymptotic forms of the probability densities

$$\begin{aligned} &p(\gamma_\alpha) \approx \exp\left[-\left(\frac{\gamma_\alpha}{\alpha'}\right)^{\alpha'}\right]; \quad \left(\frac{\gamma_\alpha}{\alpha'}\right)^{\alpha'} \gg 0; \quad \frac{1}{\alpha'} + \frac{1}{\alpha} = 1 \\ &p(\gamma_\alpha) \approx (-\gamma_\alpha)^{-\alpha-1}; \qquad \gamma_\alpha \ll 0; \qquad 0 < \alpha < 2 \end{aligned} \tag{17}$$

where the key point is that the auxiliary variable α' changes sign at $\alpha = 1$. This means that $(\gamma_\alpha/\alpha')^{\alpha'} \gg 0$ is valid for $\gamma_\alpha \gg 1$ when $\alpha > 1$, whereas for $\alpha < 1$, it is valid when $|\gamma_\alpha| \approx 0$. Note that exact closed form expressions for the probabilities of extremals only exist in the "inverse Gaussian" $\alpha = 1/2$ case; analytic symmetric Levy's exists for the $\alpha = 1$ (Cauchy) and $\alpha = 2$ (Gaussian) cases.

Now consider the noise $\gamma(\underline{x})$, produced by putting i.i.d. extremal Levy distributions onto a grid and shrinking the grid size to zero (with an appropriate normalization). This is possible because Levy distributions are "infinitely divisible"; see (Feller, 1971) (for the noise we drop the subscript α). With this noise and with the normalization constant N_D and weight function $g(\underline{x})$, Γ can be constructed as a convolution

$$\Gamma_\lambda(\underline{x}) = C_1^{1/\alpha} N_D^{-1/\alpha} \int_{1 \le |\underline{x}| \le \lambda} g(\underline{x} - \underline{x}') \gamma(\underline{x}') d^D \underline{x}' \tag{18}$$

when $\alpha < 2$, g must be non-negative otherwise Γ would a (nonextremal) mixture of extremal and nonextremal Levy variables. The constant N_D is introduced for convenience; it will allow us to always take g as an (asymptotically) unit amplitude power law as shown below. Note that in this paper we will only consider isotropic D dimensional multifractals, the only exception being the asymmetric causal processes needed in space-time simulations (Section 3.2.1). From Eq. (18), we see that the statistics of Γ are independent of $\underline{x}$, so that we can take $\underline{x} = 0$ and apply the additivity of the SCF (Eq. (15))

$$K_\Gamma(q) = \log \langle e^{q\Gamma_\lambda} \rangle = \frac{C_1}{\alpha - 1} q^\alpha N_D^{-1} \int_{1 < |\underline{x}'| < \lambda} g(\underline{x}')^\alpha d^D \underline{x}' \tag{19}$$

Since $\langle \varepsilon_\lambda^q \rangle = e^{K_\Gamma(q)}$, we see that if the SCF of Γ, $K_\Gamma(q) = K(q) \log \lambda$, then $\varepsilon_\lambda = \varepsilon^{\Gamma_\lambda}$ will have the desired statistics (Eq. (1)). In order to obtain the required log divergence for K_Γ, it suffices to choose g to be a cut-off, isotropic singularity

$$\begin{aligned} g(\underline{x}) &= |\underline{x}|^{-D/\alpha}; \quad |\underline{x}| \ge 1 \\ g(\underline{x}) &= 0 \qquad\qquad |\underline{x}| < 1 \end{aligned} \tag{20}$$

so that

$$\langle \varepsilon_\lambda^q \rangle = \langle e^{q\Gamma_\lambda} \rangle = e^{(C_1/\alpha - 1) q^\alpha N_D^{-1} \Omega_D \log \lambda}; \Omega_D = \int_{|\underline{x}| = 1} d^D \underline{x} \tag{21}$$

where Ω_D is the integral over all the angles in the D dimensional space (e.g. $\Omega_1 = 2$, $\Omega_2 = 2\pi$, $\Omega_3 = 4\pi$, etc.).

3.1.2. Normalization

From Eq. (21), we see that if we choose

$$N_D = \Omega_D \tag{22}$$

then we obtain the desired nonlinear part of the multiscaling behaviour

$$\langle \varepsilon_{\lambda,u}^q \rangle = \lambda^{K_u(q)}; \quad K_u(q) = \frac{C_1}{\alpha - 1} q^\alpha \tag{23}$$

where K_u is the unnormalized exponent scaling function corresponding to the fact that ε given by Eq. (21) is unnormalized (hence, we temporarily add the subscript "u"). A normalized $\varepsilon_{\lambda,n}$ can now be easily obtained using

$$\varepsilon_{\lambda,n} = \frac{\varepsilon_{\lambda,u}}{\langle \varepsilon_{\lambda,u} \rangle} \tag{24}$$

so that

$$\langle \varepsilon_{\lambda,n}^q \rangle = \lambda^{K(q)}; \quad K(q) = K_u(q) - q K_u(1) = \frac{C_1}{\alpha - 1}(q^\alpha - q) \tag{25}$$

as required (we temporarily add the subscript "n" to distinguish it from the unnormalized process). The above leads to cascades with the correct statistics at the finest resolution λ; unfortunately, we will now see that without corrections the internal structure of the realizations is not perfectly scaling.

3.2. Two point statistics, the second characteristic function of the log autocorrelation and its spatial part $S(\Delta x)$

3.2.1. The general problem

A simple way to examine the scaling properties of realizations of cascades developed over a finite scale ratio, Λ, is to consider two point statistics such as autocorrelation functions, or their Fourier transforms, spectra. To calculate these, we first consider the random variables: from Eq. (18) we obtain

$$\begin{aligned} (\varepsilon_\lambda(\underline{x}')\varepsilon_\lambda(\underline{x}' - \underline{\Delta x}))^q &= e^{q(\Gamma(\underline{x}') + \Gamma(\underline{x}' - \underline{\Delta x}))} \\ &= e^{q C_1^{1/\alpha} N_D^{-1/\alpha} \int_{1 \le |\underline{x}| \le \lambda} (g(\underline{x}' - \underline{x}'') + g(\underline{x}' - \underline{\Delta x} - \underline{x}'')) \gamma(\underline{x}'') d^D \underline{x}''} \end{aligned} \tag{26}$$

Hence, we see that $\Gamma(\underline{x}'') + \Gamma(\underline{x}' - \underline{\Delta x})$ is the generator of the autocorrelation. For the statistics, we can define the SCF of the generator by taking ensemble averages of the above

$$\log \langle (\varepsilon_\lambda(\underline{x}')\varepsilon_\lambda(\underline{x}' - \underline{\Delta x}))^q \rangle = \log \langle e^{q(\Gamma(\underline{x}') + \Gamma(\underline{x}' - \underline{\Delta x}))} \rangle = \frac{C_1}{\alpha - 1} q^\alpha N_D^{-1} S(\underline{\Delta x}) \tag{27}$$

the entire expression is the full SCF of the log of the autocorrelation, the key function $S(\underline{\Delta x})$ is its spatial part. Note that we do not need the more complex full two point SCF $\log \langle \varepsilon_\lambda^{q_1}(\underline{x}_1) \varepsilon_\lambda^{q_2}(\underline{x}_2) \rangle$. Using the statistical translational invariance of the process (by construction the noise "subgenerator" $\gamma_\alpha(\underline{x})$ is statistically independent of $\underline{x}$), we can take $\underline{x}' = 0$ to obtain

$$\begin{aligned} S(\underline{\Delta x}) &= \int_{1 \le |\underline{x}''| \le \lambda} (g(-\underline{x}'') + g(-\underline{x}'' - \underline{\Delta x}))^\alpha d\underline{x}'' \\ &= \int_{1 \le |\underline{x}| \le \lambda} (g(\underline{x}) + g(\underline{x} - \underline{\Delta x}))^\alpha d\underline{x} \end{aligned} \tag{28}$$

where in the far right, we have taken $\underline{x} = -\underline{x}''$ and used the fact that the domain of integration (but not necessarily g) is invariant under inversion. We have considered isotropic multifractals in a D-dimensional space; for anisotropic multifractals, we must replace the vector norm in the above by the corresponding scale function (see (Pecknold et al., 1996; Pecknold et al., 1993) for anisotropic simulations; the extension of the present technical discussion to anisotropic cascades will be made in future publications). We note that from its definition (and assumed statistical translational invariance, i.e. independence from $\underline{x}'$ in Eq. (27)), the autocorrelation function (and hence S) is symmetric under inversion: $S(\underline{\Delta x}) = S(-\underline{\Delta x})$. Isotropic processes are symmetric under rotation, in which case S is simply a function of the vector norm $|\underline{\Delta x}|$. In this case, comparing Eqs. (5), (23) and (27),

Please cite this article as: Lovejoy, S., Schertzer, D., On the simulation of continuous in scale universal multifractals, part I: Spatially continuous processes. Computers and Geosciences (2010), doi:10.1016/j.cageo.2010.04.010

we see that the theoretical $S(\underline{\Delta x})$ is

$$S(\underline{\Delta x}) = N_D \frac{\alpha-1}{C_1} \log \langle \varepsilon(\underline{x})\varepsilon(\underline{x}-\underline{\Delta x})\rangle = -N_D(2^\alpha-2)\log|\underline{\Delta x}| + N_D 2^\alpha \log\lambda \quad (29)$$

where we have used $\log\langle \varepsilon_\lambda^2\rangle = C_1/(\alpha-1)2^\alpha\log\lambda$ (Eq. (23)); the corresponding $\log\lambda$ term is absent in the normalized autocorrelation function.

3.2.2. The general $D=1$ case

For simplicity, we start with the problem in one dimension. Due to the inversion symmetry of $S(\underline{\Delta x})$ noted above, in 1-D it is sufficient to consider $\Delta x > 0$. The general $D=1$ case is

$$S(\Delta x) = \int_{1<|x|<\lambda} (g(x)+g(x-\Delta x))^\alpha dx = \int_1^\lambda [(g(x)+g(x-\Delta x))^\alpha + (g(-x)+g(-x-\Delta x))^\alpha]dx \quad (30)$$

The two basic cases of interest are the symmetric acausal case with $g(x)=g(-x)$, and the causal case with $g(x)=0$ for $x<0$ (see Marsan et al. (1996)). The corresponding condition for a space-time processes in $D+1$ dimensions to be causal is $g(\underline{x},t)=0$, $t<0$, where $\underline{x}$ is a D dimensional (spatial) vector (see part II for numerical implementations).

For the symmetric acausal case, we have

$$S(\Delta x) = \int_1^\lambda [(g(x)+g(x-\Delta x))^\alpha + (g(x)+g(x+\Delta x))^\alpha]dx \quad (31)$$

We have already seen that in this case with g a truncated power law given in Eq. (20), the normalization factor $N_D=2$ (Eqs. (21) and (22)).

For the causal case, since $g(x)=0$ for $x<0$, we have

$$S(\Delta x) = \int_1^\lambda (g(x)+g(x-\Delta x))^\alpha dx \quad (32)$$

Here, it is easy to see that the corresponding normalization factor is simply $N_D=1$.

3.2.3. The acausal $\alpha=2$, $D=1$ case

In this paper, we consider primarily the isotropic cases; in 1-D, this is the symmetric acausal case; we shall see that it generalizes directly to the higher dimensional isotropic cases. As a pedagogical example, it is useful to first consider the $\alpha=2$ case, which (with $\alpha=1/2$, 1) are the only fully analytically tractable ones (note the $\alpha=1$ case is actually a function of $x\log x$ not x, see Eq. (4)).

We take g as a symmetric singularity, cutoff for $|x|<1$; this is easy to implement numerically by using an odd integer grid (see Section 4 below)

$$g(x) = \begin{cases} |x|^{-D/\alpha}; & |x|\geq 1 \\ 0; & |x|<1 \end{cases}; \quad D=1; \quad \alpha=2 \quad (33)$$

This leads to

$$S(\Delta x) = 2\int_1^\lambda \frac{dx}{x} + \left(\int_1^{\Delta x-1}\frac{dx}{\Delta x-x} + \int_{\Delta x+1}^\lambda \frac{dx}{x-\Delta x}\right) + \int_1^\lambda \frac{dx}{x+\Delta x} + 2\int_1^{\Delta x-1}\frac{dx}{\sqrt{x(\Delta x-x)}} + 2\int_{\Delta x+1}^\lambda \frac{dx}{\sqrt{x(x-\Delta x)}} + 2\int_1^\lambda \frac{dx}{\sqrt{x(x+\Delta x)}}$$

evaluating the integrals, we obtain

$$S(\Delta x) = 2\pi + 8\log\lambda - 4\log(\Delta x + 2\sqrt{1+\Delta x}+2) - 8\tan^{-1}\frac{1}{\sqrt{\Delta x-1}} + \log\left(1-\left(\frac{\Delta x}{\lambda}\right)^2\right) + 4\left[\log\left(1+\sqrt{1-\frac{\Delta x}{\lambda}}\right) + \log\left(1+\sqrt{1+\frac{\Delta x}{\lambda}}\right)\right] \quad (34)$$

Making series expansions in Eq. (34), we obtain

$$S(\Delta x) = 2\pi + 8\log 2 + 8\log\lambda - 4\log\Delta x - 16\Delta x^{-1/2} - \frac{6}{5}\Delta x^{-5/2} + O(\Delta x^{-9/2}) - \frac{7}{4}\left(\frac{\Delta x}{\lambda}\right)^2 - \frac{99}{128}\left(\frac{\Delta x}{\lambda}\right)^4 + O\left(\frac{\Delta x}{\lambda}\right)^6 \quad (35)$$

Taking $\lambda > \Delta x \gg 1$, we see that as expected (Eq. (29)) the leading term is $-N_D(2^\alpha-2)\log|\underline{\Delta x}| = -4\log|\underline{\Delta x}| + 8\log\lambda$ with the leading correction $-16\Delta x^{-1/2}$, which comes from the $\tan^{-1}$ term and the first log term. This correction is quite large; it dominates the $\log\Delta x$ term until $\Delta x > 5$, and even when $\Delta x = 100$, it is 10% of the value.

3.2.4. The acausal 1-D $\alpha<2$ case

Considering the symmetric acausal case in 1-D (Eq. (31)) and putting the cut-off in g at $x=\pm 1$ explicitly into the limits of integration, we obtain

$$S(\Delta x) = \int_1^{\Delta x-1}[(g(x)+g(x-\Delta x))^\alpha]dx + \int_{\Delta x+1}^\lambda [(g(x)+g(x-\Delta x))^\alpha]dx + \int_1^\lambda [(g(x)+g(x+\Delta x))^\alpha]dx \quad (36)$$

This can be rewritten as follows

$$S(\Delta x) = \int_1^{\Delta x/2} g(x)^\alpha\left(1+\frac{g(\Delta x-x)}{g(x)}\right)^\alpha dx + \int_{\Delta x/2}^{\Delta x-1} g(\Delta x-x)^\alpha\left(1+\frac{g(x)}{g(\Delta x-x)}\right)^\alpha dx + \int_{\Delta x+1}^\lambda g(x-\Delta x)^\alpha\left(1+\frac{g(x)}{g(x-\Delta x)}\right)^\alpha dx + \int_1^\lambda g(x)^\alpha\left(1+\frac{g(x+\Delta x)}{g(x)}\right)^\alpha dx \quad (37)$$

so that if g is a decreasing function of $|x|$, then each ratio in the above is <1 over the indicated ranges and the binomial expansion can be used.

If we take g as a symmetric power law (Eq. (33)), then, the above integrals can be conveniently approached, using the following transformation of variables:

$$r = \frac{x}{\Delta x-x}; \quad r = \frac{\Delta x-x}{x}; \quad r = \frac{x-\Delta x}{x}; \quad r = \frac{x}{x+\Delta x} \quad (38)$$

leading (respectively, term by term) to the following

$$S(\Delta x) = \int_{1/(\Delta x-1)}^1 (1+r^{1/\alpha})^\alpha \frac{dr}{r(1+r)} + \int_{1/(\Delta x-1)}^1 (1+r^{1/\alpha})^\alpha \frac{dr}{r(1+r)} + \int_{1/(\Delta x+1)}^{1-\Delta x/\lambda} (1+r^{1/\alpha})^\alpha \frac{dr}{r(1-r)} + \int_{1/(\Delta x+1)}^{(1+\Delta x/\lambda)^{-1}} (1+r^{1/\alpha})^\alpha \frac{dr}{r(1-r)} \quad (39)$$

Rearranging, we obtain

$$S(\Delta x) = 4\int_{\Delta x^{-1}}^{(1+\Delta x/\lambda)^{-1}} (1+r^{1/\alpha})^\alpha \frac{dr}{r(1-r^2)} + 2\int_{(1+\Delta x/\lambda)^{-1}}^1 (1+r^{1/\alpha})^\alpha \frac{dr}{r(1+r)} - \int_{(1+\Delta x/\lambda)^{-1}}^{1-\Delta x/\lambda} (1+r^{1/\alpha})^\alpha \frac{dr}{r(1-r)} + O(\Delta x^{-2}); \quad (40)$$

Please cite this article as: Lovejoy, S., Schertzer, D., On the simulation of continuous in scale universal multifractals, part I: Spatially continuous processes. Computers and Geosciences (2010), doi:10.1016/j.cageo.2010.04.010

We have also used (for $\Delta x \gg 1$) the approximation $(1 \pm \Delta \underline{x})^{-1} = \Delta x^{-1} \pm \Delta x^{-2} +, \ldots$. Hence using $(1 \pm \Delta x)^{-1} \approx \Delta x^{-1}$, there will be corrections of order Δx^{-2}. Also, it can be seen that the last two integrals cancel to first order in $\Delta x/\lambda$, so that they are of order $(\Delta x/\lambda)^2$ (indeed, due to the evenness of g, the analytic terms in S are symmetric, so that they are also even).

We therefore obtain the key result

$$S(\Delta x) = 2N_D \int_{\Delta x^{-1}}^{(1+\Delta x/\lambda)^{-1}} (1+r^{D/\alpha})^{\alpha} \frac{dr}{r(1-r^2)} + O(\Delta x^{-2}) + O(\Delta x/\lambda)^2; \quad D=1; \quad N_1 = 2 \tag{41}$$

with the normalization factor $N_1 = 2$ in $D = 1$ dimensions. We have written the leading expression for S in this more general form (with $r^{D/\alpha}$ in place of $r^{1/\alpha}$), since will see that with $\Delta x = |\underline{\Delta x}|$ the same formula holds for the higher dimensional isotropic cases.

We note that for $\Delta x \gg 1$ and $\lambda \gg \Delta x$ that the lower and upper limits of integration are, respectively, near the $r=0$, $r=1$ singularities of the integrand, so that to estimate the integral, we must use separate expansions around each of the singularities. (the common region of convergence is the unit interval with endpoints removed). Hence, we can exploit the common point $r = 1/2$ to define the following functions

$$\begin{aligned} I_-(r,\alpha,D) &= \int_r^{1/2} \frac{dr'}{r'} \left(\frac{(1+r'^{D/\alpha})^{\alpha}}{(1-r'^2)} - 1 \right) \\ &= B_-(\alpha,D) - \frac{\alpha^2}{D} r^{D/\alpha} - \frac{\alpha^2(\alpha-1)}{2D} r^{2D/\alpha} + O(r^{2D/\alpha+1}) \\ &\quad + 2^{-1} r^2 + O(r^{D/\alpha+2}) \qquad 0 \le r < 1 \end{aligned}$$

$$\begin{aligned} I_+(r,\alpha,D) &= \frac{1}{2} \int_{1/2}^{r} \frac{dr'}{(1+r')} \frac{(1+r'^{D/\alpha})^{\alpha}}{r'} \\ &\quad + \frac{1}{2} \int_{1/2}^{r} \frac{dr'}{(1-r')} \left(\frac{(1+r'^{D/\alpha})^{\alpha}}{r'} - 2^{\alpha} \right) \\ &= B_+(\alpha,D) + 2^{\alpha-2}(1+D)(1-r) \\ &\quad + 2^{\alpha-4} \left(14 + 8D - D^2 \left(1 + \frac{1}{\alpha} \right) \right) (1-r)^2 + O(1-r)^3 \\ &\quad 0 < r \le 1 \end{aligned} \tag{42}$$

where $B_{\pm}(\alpha, D)$ are only dependent on α, D.

Using these definitions and expansions, we finally obtain

$$\begin{aligned} S(\Delta x) &= 2N_D \begin{bmatrix} I_-(\Delta x^{-1},\alpha,D) - \log \Delta x^{-1} + I_+((1+\Delta x/\lambda)^{-1},\alpha,D) \\ -2^{\alpha-1} \log(1-(1+\Delta x/\lambda)^{-1}) \end{bmatrix} \\ &= C(\alpha,D) - N_D \left[(2^{\alpha}-2) \log \Delta x - 2^{\alpha} \log \lambda + 2 \frac{\alpha^2}{D} \Delta x^{-D/\alpha} \right] \\ &\quad - O(\Delta x^{-2}) + O(\Delta x^{-2m-nD/\alpha}) + O\left(\frac{\Delta x}{\lambda} \right)^2 \end{aligned} \tag{43}$$

where $C = 2N_D(B_- + B_+)$ is constant with respect to Δx, λ and is unimportant; n and m are positive integers and $D = 1$, $N_1 = 2$. The leading order expression for S is thus $= -N_D(2^{\alpha}-2)(\log \Delta x) + N_D 2^{\alpha} \log \lambda$ as expected (Eq. (29)) with the leading Δx dependent correction $-2N_D(\alpha^2/D)\Delta x^{-D/\alpha}$.

Using the above expansion for $S(\Delta x)$, we can obtain the following expression for the autocorrelation function

$$\langle \varepsilon(x)\varepsilon(x-\Delta x) \rangle \propto \Delta x^{-K(2)} \exp\left(-\frac{2C_1}{D} \frac{\alpha^2}{\alpha-1} \Delta x^{-D/\alpha} \right) \tag{44}$$

where we have only kept the $(\Delta x^{-D/\alpha})$ correction to the leading power law term. To gauge the importance of this correction, Fig. 7 shows the behaviour for $D = 1$, with C_1 having the moderate value

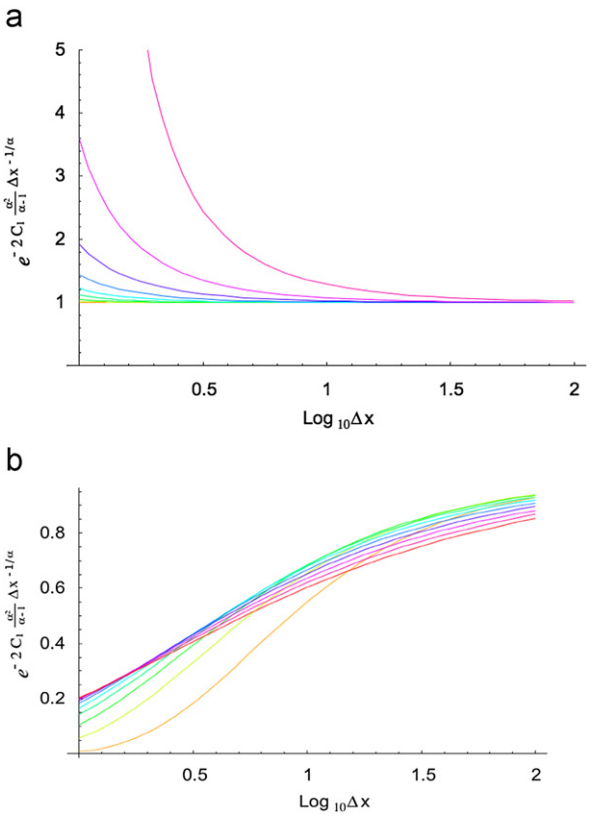

Fig. 7. (a) Corrections for $D = 1$ case, $\alpha < 1$, normalized correctly and using $C_1 = 0.2$. α increasing from left to right in increments of 0.1 red (far right) is 0.9. (b) Same but for $\alpha > 1$, orange is $\alpha = 1.1$, red, $\alpha = 2$. (For interpretation of the references to color in this figure legend, the reader is referred to the web version of this article.)

0.2. We see that as expected, the effect is particularly strong for the larger α, and that for Δx as large as 100 it can still be a 10% effect.

3.2.5. The 1-D causal case

Starting with Eq. (32) for the causal $S(\Delta x)$, we may explicitly take into account the truncation in g at $x = 1$ by changing the range of integration

$$S(\Delta x) = \int_1^{\Delta x - 1} (g(x))^{\alpha} dx + \int_{\Delta x+1}^{\lambda} (g(x) + g(x-\Delta x))^{\alpha} dx; \quad \Delta x > 0 \tag{45}$$

with

$$g(x) = \begin{matrix} x^{-1/\alpha}; & x > 1 \\ 0; & x < 1 \end{matrix}; \quad D = 1 \tag{46}$$

Using the transformation of variables $r = x - \Delta x/x$, we obtain

$$S(\Delta x) = \log(\Delta x - 1) + \int_{(\Delta x+1)^{-1}}^{(1+\Delta x/\lambda)^{-1}} (1+r^{1/\alpha})^{\alpha} \left(\frac{1}{r} + \frac{1}{1-r} \right) dr; \quad \Delta x > 1 \tag{47}$$

we see that to within terms of $O(1/\Delta x)$ this is half the value of the previous acausal expression (Eq. (41)). However, we saw in Section 3.2.1 that the N_D for the causal case was half that of the acausal one so that after normalization by N_D, the $\log \Delta x$ and $\Delta x^{-1/\alpha}$ terms are the same, the main difference is that there will now be Δx^{-1} terms (previously they cancelled by symmetry of the $g(x)$).

Please cite this article as: Lovejoy, S., Schertzer, D., On the simulation of continuous in scale universal multifractals, part I: Spatially continuous processes. Computers and Geosciences (2010), doi:10.1016/j.cageo.2010.04.010

4. Conclusions

There is a growing body of evidence suggesting that geofields are generally multifractal over at least some (possibly very large) range of space-time scales. This motivates the development of techniques for their simulation. While realistic applications are invariably continuous in scale, most multifractal simulations used in the literature are discrete-in-scale multiplicative cascades, in which integer scale ratios and their integer powers play special roles leading to simulations dominated with straight line or planar artifacts (in 2-D and 3-D).

To make the cascades continuous in scale, the basic noise must be "infinitely divisible"; the choice considered here being Levy noises (index α), which have the additional interest of being the stable, attractive (hence "universal") cascade processes: they arise as a consequence of a kind of "multiplicative central limit theorem". In this first part, we consider the basic (theoretical) continuous in space, continuous in scale process proposed by Schertzer and Lovejoy (1987) (developed further in Wilson et al., 1991; Marsan et al., 1996; Pecknold et al., 1997), with extensions to causal space-time processes. Although the original method works, convergence to the theoretical statistical behaviour can be slow, sometimes requiring very significant ranges of scale. In order to quantify these issues and to develop improvements, we considered two point statistics (autocorrelations, their SCF and spectra). We found that in addition to the desired power law correlations $\Delta x^{-K(2)}$, there are spurious correlations, which only decay slowly (of the form $\exp(-A\Delta x^{-D/\alpha})$, where D is the dimension of space; there are also other terms, but this is the most important (especially for $2 \geq \alpha > 1$). These deviations are examples of "finite size effects," since they disappear for $\Delta x \gg 1$. We also found large scale deviations when $\Delta x/\lambda \approx 1$, but these were less important. In part II, we explore the consequences of spatial discretisation and show how to remove the leading deviation term for isotropic causal and acausal processes.

Acknowledgements

One of the authors (SL) would like to thank the Laboratoire de Modelisation en Méchanique for hosting a sabbatical, where much of this work was done. This work was done for scientific purposes only, it was unfunded.

References

Basu, S., Foufoula-Georgiou, E., Porté-Agel, F., 2004. Synthetic turbulence, fractal interpolation and large-eddy simulations. Physical Review E 70, 026310–026313.
Cahalan, R., 1994. Bounded cascade clouds: albedo and effective thickness. Nonlinear Processes in Geophysics 1, 156–167.
Calvet, L.E., Fisher, A.J., 2001. Forecasting multifractal volatility. Journal of Econometrics 105, 27–58.
Calvet, L.E., Fisher, A.J., 2008. "Multifractal Volatility" theory, Forecasting and Pricing. Academic Press, New York 258pp.
Cheng, Q., Agterberg, F., 1996. Multifractal modelling and spatial statistics. Mathematical Geology 28, 1–16.
Feller, W., 1971. An Introduction to Probability Theory and its Applications, vol. 2. Wiley, New York 669pp.
Kolmogorov, A.N., 1941. Local structure of turbulence in an incompressible liquid for very large Reynolds numbers. (English translation: Proceedings of the Royal Society A434, 9–17, 1991). In: Proceedings of the Academy of Sciences of the USSR, Geochemistry Section 30, 299–303.
Laferrière, A., Gaonac'h, H., 1999. Multifractal properties of visible reflectance fields from basaltic volcanoes. Journal of Geophysical Research 104, 5115–5126.
Levy-Véhel, J., Daoudi, K., Lutton, E., 1995. Fractal modeling of speech signals. Fractals 2, 379–382.
Lovejoy, S., Schertzer, D., 2007. Scaling and multifractal fields in the solid earth and topography. Nonlinear Processes in Geophysics 14, 1–38.
Lovejoy, S., Schertzer, D., 2010a. Towards a new synthesis for atmospheric dynamics: space-time cascades. Atmospheric Research 96, 1–52. doi:10.1016/j.atmosres.2010.1001.1004.
Lovejoy, S., Schertzer, D., 2010b. Multifractal Cascade Processes and the Emergence of Turbulent Laws in the Atmosphere. Cambridge University Press (in press).
Lovejoy, S., Schertzer, D., Allaire, V., Bourgeois, T., King, S., Pinel, J., Stolle, J., 2009a. Atmospheric complexity or scale by scale simplicity? Gseophysical Research Letters 36 L01801, doi:01810.01029/02008GL035863.
Lovejoy, S., Tuck, A.F., Hovde, S.J., Schertzer, D., 2009b. The vertical cascade structure of the atmosphere and multifractal drop sonde outages. Journal of Geophysical Research 114, D07111, doi:07110.01029/02008JD010651.
Lovejoy, S., Tuck, A., Schertzer, D., 2010. The Horizontal cascade structure of atmospheric fields determined from aircraft data. Journal of Geophysical Research 115, D13105, doi:10.1029/2009JD013353.
Mandelbrot, B.B., 1974. Intermittent turbulence in self-similar cascades: divergence of high moments and dimension of the carrier. Journal of Fluid Mechanics 62, 331–350.
Marsan, D., Schertzer, D., Lovejoy, S., 1996. Causal space-time multifractal processes: predictability and forecasting of rain fields. Journal of Geophysical Research 31D, 26333–26346.
Monin, A.S., Yaglom, A.M., 1975. Statistical Fluid Mechanics. MIT press, Boston MA 676pp.
Novikov, E.A., Stewart, R., 1964. Intermittency of turbulence and spectrum of fluctuations in energy-disspation. Izvestiya Akademii Nauk SSSR. Serie Geofizica 3, 408–412.
Pecknold, S., Lovejoy, S., Schertzer, D., 1996. The morphology and texture of anisotropic multifractals using generalized scale invariance. In: Woyczynski, W., Molchansov, S. (Eds.), Stochastic Models in Geosystems. Springer-Verlag, New York, pp. 269–312.
Pecknold, S., Lovejoy, S., Schertzer, D., Hooge, C., 1997. Multifractals and the resolution dependence of remotely sensed data: generalized scale invariance and geographical information systems. In: Quattrochi, M.G.D. (Ed.), Scaling in Remote Sensing and Geographical Information Systems. Lewis, Boca Raton, Florida, pp. 361–394.
Pecknold, S., Lovejoy, S., Schertzer, D., Hooge, C., Malouin, J.F., 1993. The simulation of universal multifractals. In: Perdang, J.M., Lejeune, A. (Eds.), Cellular Automata: Prospects in Astronomy and Astrophysics. World Scientific, Singapore, pp. 228–267.
Schertzer, D., Lovejoy, S., 1985a. Generalised scale invariance in turbulent phenomena. Physico-chemical Hydrodynamics Journal 6, 623–635.
Schertzer, D., Lovejoy, S., 1985b. The dimension and intermittency of atmospheric dynamics. In: Launder, B. (Ed.), Turbulent Shear Flow, vol. 4. Springer-Verlag, pp. 7–33.
Schertzer, D., Lovejoy, S., 1987. Physical modeling and analysis of rain and clouds by anisotropic scaling of multiplicative processes. Journal of Geophysical Research 92, 9693–9714.
Schertzer, D., Lovejoy, S., 1997. Universal multifractals do exist!. Journal of Applied Meteorology 36, 1296–1303.
Schertzer, D., Lovejoy, S., Schmitt, F., 1995. Structures in turbulence and multifractal universality. In: Meneguzzi, M., Pouquet, A., Sulem, P.L. (Eds.), Small-Scale Structures in 3D and MHD Turbulence. Springer-Verlag, New York, pp. 137–144.
She, Z.S., Levesque, E., 1994. Universal scaling laws in fully developed turbulence. Physical Review Letters 72, 336–339.
Wilson, J., Schertzer, D., Lovejoy, S., 1991. Physically based modelling by multiplicative cascade processes. In: Schertzer, D., Lovejoy, S. (Eds.), Non-Linear Variability in Geophysics: Scaling and Fractals. Kluwer, Dordrecht, The Netherlands, pp. 185–208.
Yaglom, A.M., 1966. The influence on the fluctuation in energy dissipation on the shape of turbulent characteristics in the inertial interval. Soviet Physics Doklady 2, 26–30.

Please cite this article as: Lovejoy, S., Schertzer, D., On the simulation of continuous in scale universal multifractals, part I: Spatially continuous processes. Computers and Geosciences (2010), doi:10.1016/j.cageo.2010.04.010